

Underwater Variable Zoom: Depth-Guided Perception Network for Underwater Image Enhancement

Zhixiong Huang, Xinying Wang, Jinjiang Li, Shenglan Liu, Lin Feng*

Abstract—Underwater scenes intrinsically involve degradation problems owing to heterogeneous ocean elements. Prevailing underwater image enhancement (UIE) methods stick to straightforward feature modeling to learn the mapping function, which leads to limited vision gain as it lacks more explicit physical cues (e.g., depth). In this work, we investigate injecting the depth prior into the deep UIE model for more precise scene enhancement capability. To this end, we present a novel depth-guided perception UIE framework, dubbed underwater variable zoom (UVZ). Specifically, UVZ resorts to a two-stage pipeline. First, a depth estimation network is designed to generate critical depth maps, combined with an auxiliary supervision network introduced to suppress estimation differences during training. Second, UVZ parses near-far scenarios by harnessing the predicted depth maps, enabling local and non-local perceiving in different regions. Extensive experiments on five benchmark datasets demonstrate that UVZ achieves superior visual gain and delivers promising quantitative metrics. Besides, UVZ is confirmed to exhibit good generalization in some visual tasks, especially in unusual lighting conditions. The code, models and results are available at: <https://github.com/WindySprint/UVZ>.

Index Terms—Underwater image enhancement, Depth-guided perception, Near-far scenarios, Color correction.

I. INTRODUCTION

As a crucial information carrier, underwater images play an important role in ocean tasks[1]. Unfortunately, underwater images often encounter various degradation problems due to two main factors [2]. Firstly, different wavelengths of light decay at varying rates in the underwater medium, resulting in a prevalent blue-green color deviation. Secondly, the scattering effect of suspended particles hinders normal light propagation, leading to problems such as low contrast and blurred details [3]. Meanwhile, these degradations worsen with the increasing distance from the imaging scene to the camera [4]. Therefore, underwater image enhancement (UIE) methods have been widely applied to improve vision quality, highlighting important practical value.

Z. Huang and X. Wang are with the School of Computer Science and Technology, Dalian University of Technology, Dalian 116024, China (e-mail: hzxcyanwind@mail.dlut.edu.cn; wangxinying@mail.dlut.edu.cn).

J. Li is with the School of Computer Science and Technology, Shandong Technology and Business University, Yantai 264005, China (e-mail: lijijiang@gmail.com).

S. Liu is with the School of Innovation and Entrepreneurship, Dalian University of Technology, Dalian 116024, China (e-mail: liusl@dlut.edu.cn).

L. Feng is with the School of Information and Communication Engineering, Dalian Minzu University, 116600 Dalian 116600 Liaoning, China, and also with the School of Innovation and Entrepreneurship, Dalian University of Technology, Dalian 116024, China (e-mail: fenglin@dlut.edu.cn).

In the early days of UIE field, researchers have proposed model-free and model-based traditional methods. Model-free methods [5, 15, 16] enhances underwater images by modifying pixels in degraded channels and blurred regions. On the other hand, model-based methods [7, 17] introduce depth information and models to build the underwater degradation process, and reverse it to restore underwater images. In recent years, deep learning methods [11, 18, 19] have shown remarkable enhancements, leveraging benchmark data and miscellaneous networks. Despite significant progress achieved with the above methods, challenges emerge when addressing widely varying degrees of regional degradation. Fig. 1 exhibits the enhancement effects of some UIE methods on near-far scenarios. It is evident that the degradation degree varies between the near scene (orange region) and far scene (red region) in the raw image. In comparison, the visual quality of the former and the adjacent region still exhibits relatively better performance. While most methods have considerable visual improvement in the near scene, but still retain notable color deviation in the far scene. For more accurate color enhancement, we advocate that this process should incorporate depth information related to scene distance, which allows for a more precise division of different regions in underwater images.

Previous works [12, 13, 20] have incorporated depth maps to explore physical cues, contributing to the response of degraded regions. However, direct weight adjustments may restrict the exploration of visual cues, as the adjacent features of far and near points exhibit varying gains in the enhancement process. With the above analysis, we hope to construct an adaptive region enhancement method. Before enhancing each point, the depth information should be used to determine the importance of non-local and local information. In the near-field region, local information is critical to the quality of the enhanced image, whereas in the far-field region, non-local information can provide valuable insights.

To achieve adaptive learning in the near-far region, this paper proposes a novel UIE method based on depth-guided perception, UVZ, which includes depth estimation network (DEN), auxiliary supervision network (ASN), and depth-guided enhancement network (DGEN). First, the proposed model generates a depth map by DEN, and uses ASN to further supervise the rationality of the depth map during training. Meanwhile, the desired features for different regions are captured by non-local and local branches in DGEN. To adapt

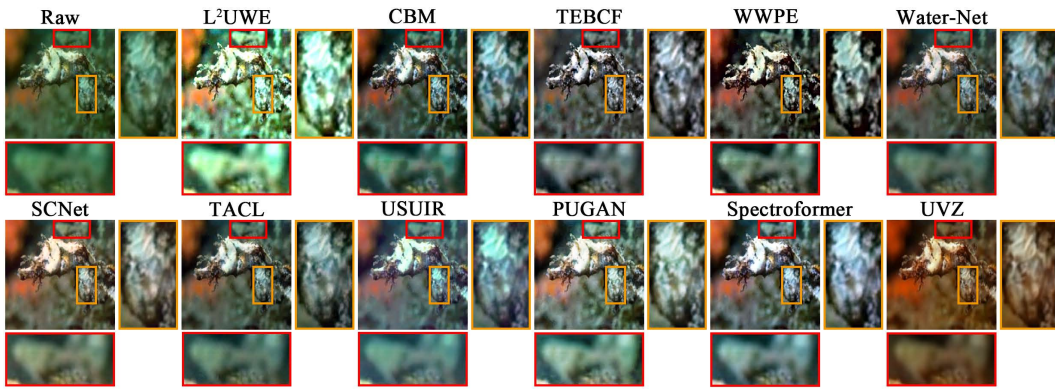


Fig. 1. Near-far scenarios enhancement comparison by different methods, where the orange box represents the enlarged near scene and the red box represents the enlarged far scene. The top row shows the raw image, the results of L²UWE [5], CBM [6], TEBCF [7], WWPE [8], and Water-Net [9]. The bottom row shows the results of SCNet [10], TACL [11], USUIR [12], PUGAN [13], Spectroformer [14], and our UVZ.

to varying receptive fields, we perform a R^3N transformation on the estimated depth map, guiding feature fusion in different regions. Through the above process, UVZ effectively and comprehensively enhances the color, contrast, and clarity of underwater images.

The main contributions of this paper are as follows:

- We designed three sub-networks to compose a new depth-guided perception framework, UVZ. For non-homogeneous degraded underwater scenes, we employ a learning strategy that adaptively combines non-local and local features.
- To enhance the ability to distinguish degraded regions, we incorporate an attention estimation-scene reconstruction training process. This step aims to strengthen the correlation between the depth map and the underwater scene.
- Compared to state-of-the-art methods, our UVZ demonstrates more attractive results in both qualitative and quantitative comparisons. Moreover, UVZ exhibits generalization abilities to other visual tasks without parameter tuning.

II. RELATED WORK

A. Traditional Methods

In response to the degradation characteristics of images, model-free methods notably enhance the contrast and saturation of the images. Ancuti et al. [15] fused color compensated and white balance images to obtain natural underwater image. Marques et al. [5] used contrast to guide the generation of images with salient details and brightness enhancement. Based on the concept of contour bougie morphology, Yuan et al. [6] enhanced the image quality by mitigating scattering blur and contrast stretching. Zhang et al. [3] introduced the attenuation characteristics to correct the color, and introduced the integral and squared integral maps to enhance the contrast. Kang et al. [21] decompose the image into mean intensity, contrast, and structure, the three components are fused in different ways to obtain the enhancement result. However, such methods overlook the characteristics of underwater degradation process, especially the depth between the object and the camera [22, 23], leading to color distortion or improper enhancement.

Model-based methods explore the process of underwater image degradation and use priors and assumptions to model

this process. Berman et al. [24] used the haze-lines model to enhance the attenuated colors. Alenezi et al. [17] introduced gradient and absorption differences associated with color channels into background light and transmission map estimation. Yuan et al. [7] enhanced the visibility of images by dark channel prior and color compensation in two color spaces, respectively. Zhou et al. [23] introduced light attenuation features and feature prior in estimating background light and transmission map. Chandrasekar et al. [25] combine underwater image formation models and depth information to remove backscatter, and utilize lightweight networks and retinex model to further enhance the image. Due to the variability of underwater environments, the parameters and priors set by these methods are limited and cannot fully adapt to specific underwater scenarios.

B. Deep Learning Methods

In recent years, deep learning methods have been widely applied in UIE due to remarkable effect. Wang et al. [26] introduced HSV space for the first time to adjust the brightness and saturation of underwater images. Jiang et al. [27] incorporated the laplacian pyramid to construct a lightweight multi-scale network, and improved the performance by recursive strategy and residual learning. Zhou et al. [18] combined RGB and HSV color spaces to enhance the underwater images, and used attention and color-guided map to guide the network to perceive critical information. Zhang et al. [28] introduced multi-level sub-networks to enrich the feature representation, and proposed a triple attention module to selectively cascade different features. By observing from the perspective of color spectrum distribution, Rao et al. [19] proposed a two-stage network using texture cues and color cues to enhance the underwater images. Wang et al. [29] integrated the wavelet transform and color compensation mechanism in the network to perform multi-level enhancement of details and colors.

To avoid the need for paired underwater images, unsupervised learning methods have received considerable attention. Jiang et al. [30] migrated image dehazing from air to the underwater domain, thus avoiding the reliance of paired underwater images. Liu et al. [11] constructed a twin adversarial

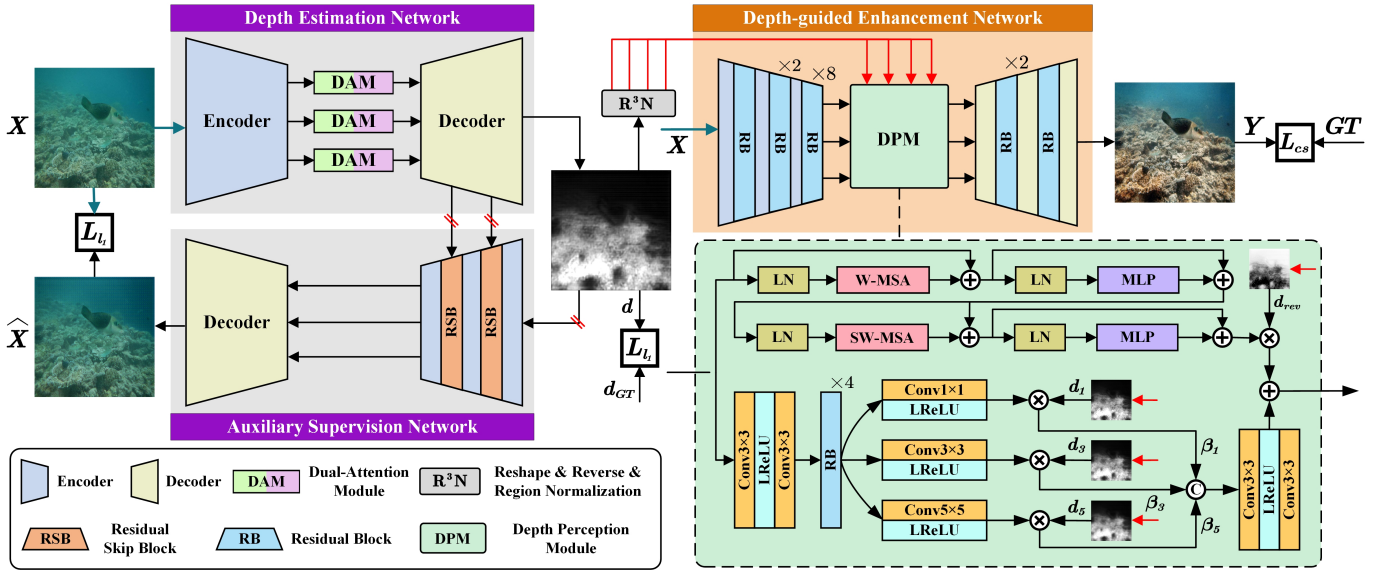


Fig. 2. The two-stage framework of UVZ, including DEN, DGEN, and ASN. All sub-networks adopt a standard encoder/decoder architecture, where the red slash indicates that ASN is only used for the training. In the first stage, for a raw image X , DEN and ASN generate the depth map d and the regression image \hat{X} , respectively. For the second stage, with inputs X and d , DGEN generates the enhanced image Y .

contrastive learning framework and utilized underwater object detection tasks to guide image enhancement. Jiang et al. [31] employed global-local adversarial mechanism to supervise image realism. Li et al. [32] introduced comparative learning into UIE and utilized the discriminator to evaluate the quality of different regions.

Due to the lack of degradation cues, relying solely on network mapping may not comprehensively enhance underwater images, resulting in residual blue-green deviations. To tackle this challenge, we introduced depth information associated with the degradation process to guide the network.

C. Depth-related Methods

The widespread application of depth information in image dehazing [33, 34, 35] has enlightened the understanding of underwater scenes in the UIE field. Zhou et al. [36] used channel intensity prior and unsupervised method to generate two depth maps, further eliminated the blurring problem caused by scattering effects. Chen et al. [20] introduced position attention and dilated convolution into the depth estimation network, guiding weight allocation by the predicted depth map. Fu et al. [12] reconstructed the raw image by predicting a depth-related transmission map, thereby obtaining the scene radiance for degradation. Cong et al. [13] used the depth map and the physical model for image restoration, with dual-discriminators constraining the generation of the restored image and the depth map. Hou et al. [37] improved the estimation of transmission map by the local background light and reflectance map, which can eliminate the influence of non-uniform light in underwater scenes.

The above method incorporates depth information to adapt degradation scenes, but low-quality features still impact the enhancement of distant regions. Considering this, we employ adaptive learning for regions at various distances, aiming to establish differentiated region enhancement.

III. METHODOLOGY

As shown in Fig. 2, UVZ constitutes a two-stage UIE framework. First, we input the raw image $X \in \mathbb{R}^{H \times W \times 3}$ to DEN with a standard encoder-decoder architecture. Within this process, a dual-attention module (DAM) is introduced to focus on severely degraded regions, thereby obtaining a depth map $d \in \mathbb{R}^{H \times W \times 1}$ with well-defined near-far regions. During the training process, we generate a regression map $\hat{X} \in \mathbb{R}^{H \times W \times 3}$ for color restoration via ASN to promote greater correlation between d and X . To refine the restoration of \hat{X} , ASN fuses the decoded features from DEN with residual skip blocks (RSB). Second, we design a depth perception module (DPM) for near-far region learning in DGEN, consisting of two branches: swin transformer [38] and multi-kernel convolution. The two branches are used for non-local and local feature learning, respectively, with selective fusion guided by d . In response to DPM, we apply an R^3N transformation on d , as presented in Fig. 3. Using the adjusted depth maps and the learnable parameters, we constructed a fusion strategy with receptive field adaptation for a more reasoned combination of non-local and local features.

A. Depth Perception Module

For most UIE networks, convolution is commonly used to capture local information over short distances. While these methods effectively eliminate most color deviation, certain regions may still be affected by blue-green, particularly in far regions with severe degradation. As the enhancement process of far point is mainly dominated by the surrounding degraded features, local feature extraction instead hinders the restoration of underwater colors. To locate regions with severe degradation, we notice the correlation between depth and degradation in the underwater imaging model. A reasonable depth map can assess the quality of different regions to a certain extent,

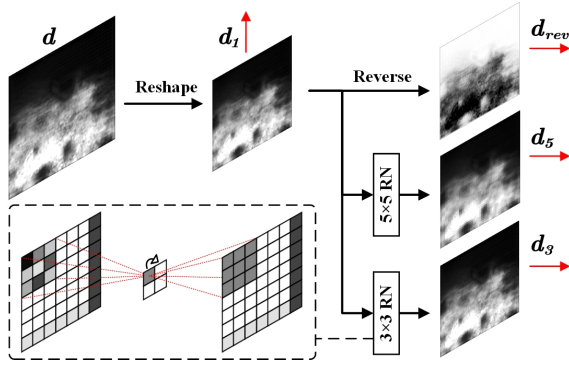


Fig. 3. R³N transformation of a depth map. The input is the depth map d and the outputs are the feature maps d_{rev} , d_1 , d_3 , and d_5 . The process within the dashed line is a 3×3 region normalization (RN).

thereby guiding a more comprehensive color enhancement. To this end, we constructed a DPM that guides perception with depth, and adaptively enhance different regions through non-local and local learning branches. DPM is illustrated in Fig. 2.

To adapt the receptive fields of the two branches, we design an R³N transformation for the depth map d , as presented in Fig. 3. First, we reshape d to $d_1 \in \mathbb{R}^{h \times w \times 1}$ consistent with the encoded feature scale, which is performed by nearest interpolation. Second, we alter the weight distribution of the near and far scenes by reversing the depth map $d_{rev} = 1 - d$, so that the non-local branch focuses more on high-quality information. In addition, through the idea of region normalization (RN) [39], we smooth the weight distribution of the degraded regions, thereby avoiding the interference of far points with higher degradation on local information capture. RN divides the regions based on the size of the convolution kernel in the local branch, calculating the mean value of each region for normalization. The specific process is as follows:

$$\begin{aligned} d_1 &= R_1 \cup R_2 \cup \dots \cup R_n, \\ \mu_i &= \frac{1}{k^2} \sum_{x_{ij} \in R_i} x_{ij}, \end{aligned} \quad (1)$$

where R_1, R_2, \dots, R_n represent the different division regions, $n = (hw)/k^2$. x_{ij} represents the j th pixel of region R_i , and all pixels in that region are represented by the mean value μ_i . Ultimately, we employ RN to obtain d_3 and d_5 corresponding to 3×3 and 5×5 convolutions. By guiding the selective fusion in DPM, the transformed depth map will enable the network to develop a reasonable perception of the degraded regions, making the enhanced colors more natural.

We adopt the swin transformer to implement non-local branch for capturing dependencies. Compared with the traditional transformer structure, the swin transformer utilizes the shifted windows to fully enhance the receptive field, further extending the non-local interaction ability. The input encoded features are first partitioned into a non-overlapping patch sequence $f_i = [p_1, p_2, \dots, p_m]$, then flattened into linear vectors and computed as follows:

$$\begin{aligned} \hat{f}_i &= MSA(LN(f_i)) + f_i, \\ f_i &= MLP(LN(\hat{f}_i)) + \hat{f}_i, \end{aligned} \quad (2)$$

where $LN(\cdot)$ represents layer normalization, and $MLP(\cdot)$ represents multi-layer perceptron. $MSA(\cdot)$ represents multi-head self-attention, which alternates between window-based and shift-window-based partitioning strategies. We merge the extracted patch sequences to obtain the feature map f_t , and multiply it with d_{rev} to obtain the non-local result $f_r = f_t \times d_{rev}$. By non-local branch, we reduce the attention to surrounding information in far regions, avoiding the poor-quality features dominating the enhancement process. Instead, high-quality features will serve as a more favorable option for the region.

On the other hand, local information should play a crucial role in near regions with good imaging. Compared to the non-local region, adjacent features tend to be more helpful for the enhancement process in that region. In the local branch, we propose a local feature extractor based on multi-kernel convolutions, including four 3×3 convolutions, four residual blocks, and three convolutions with different kernel sizes (1, 3, and 5), where the activation functions are LeakyReLU. To improve the spatial distribution perception of underwater scenes, multi-kernel convolutions are applied to obtain more perceptual fields, thereby enhancing scene details of varying sizes in multi-scale encoding features. We multiply the convolutional features f_{c1}, f_{c3}, f_{c5} with the corresponding depth maps d_1, d_3, d_5 , and dynamically adjust the weights by three learnable parameters β_1, β_3 , and β_5 :

$$f_{ck} = d_k \times f_{ck} \times \beta_k, k = 1, 3, 5 \quad (3)$$

We concatenate the three outputs on the channel dimension and generate local branch results by composite convolutional blocks. Combining the results of non-local and local branch to output the following feature $f_o \in \mathbb{R}^{h \times w \times c}$:

$$f_o = f_r + cat(f_{c1}, f_{c3}, f_{c5})_{clc}, \quad (4)$$

where $cat(\cdot)$ represents the concatenate operation on channel dimension, and $(\cdot)_{clc}$ represents the convolution-activation-convolution structure.

B. Dual-Attention Module

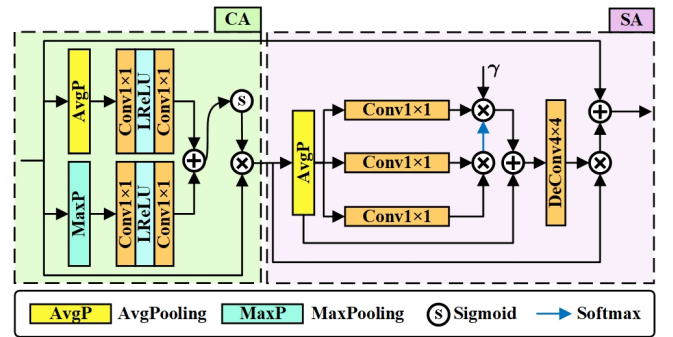


Fig. 4. Structure of the Dual-Attention Module (DAM)

In complex underwater imaging processes, the depth-related degradation attenuation is quite common. As shown in Fig. 4, we design a DAM to generate reasonable depth maps, consisting of channel attention (CA) and self-attention (SA). In

CA, we combine the convolutional results of two pooling operations to extract channel importance f_{ca} from the encoding feature f :

$$f_{ca} = f \times (AvgP(f)_{clc} + MaxP(f)_{clc})_{sig}, \quad (5)$$

where $AvgP(\cdot)$ and $MaxP(\cdot)$ represent the average pooling layer and maximum pooling layer, respectively, and $(\cdot)_{sig}$ is the sigmoid function. Next, we input the features annotated with channel weights into SA, allowing regions with different degradation degrees to have distinct weights. SA first uses the average pooling layer to reduce the scale, and then obtains spatial importance f_{sa} by the following process:

$$\begin{aligned} q &= k = v = (f_{ca})_c, \\ f_{sa} &= f_{ca} + \gamma \times ((q \times k)_s \times v), \end{aligned} \quad (6)$$

where $(\cdot)_s$ is a softmax function, and γ is a learnable parameter used to adjust the intensity. We use the deconvolution $(\cdot)_{dc}$ to reshape features into input scale and annotate spatial weights back to input features. The hidden feature f_h with regional degradation prominence is obtained by the fusion of two attention features:

$$f_h = f + f_{ca} \times (f_{sa})_{dc} \quad (7)$$

Finally, we use the decoder to generate corresponding depth maps, guiding the network to perceive different degraded regions. In various underwater scenarios, although the region division of the depth map may not be precise enough, extensive experiments have demonstrated that the UVZ has good generalization and generates results with natural colors.

C. Residual Block and Residual Skip Block

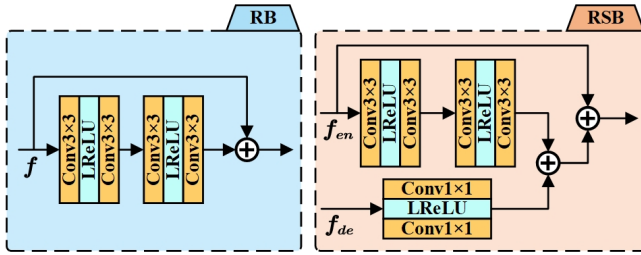


Fig. 5. Structure of the Residual Block (RB) and Residual Skip Block (RSB)

Fig. 5 shows the details of RB and RSB. In both blocks, we extract features through convolution-activation-convolution structures and residual connection, while extra 1×1 convolution blocks are applied to RSB to fuse decoded features from DEN. We add many RB to solve the gradient vanishing, and assist the ASN in generating a more complete regression image \hat{X} by RSB.

D. Training Strategy

The UVZ training process is supervised in two stages. In the first stage, we compute losses for the outputs of DEN and ASN, respectively, which is an offline pre-training process. During the second stage, we use DEN with fixed parameters to assist DGEN in generating the enhanced image, thereby obtaining relevant losses. The first stage of training is conducted

by synthesized dataset [40], which contains underwater images and corresponding depth maps of five open ocean waters and coastal waters. We randomly selected 600 image pairs to train DEN and ASN for 100 epochs, and calculated the following l_1 loss:

$$L_{l_1} = \frac{\lambda_1}{hw} \sum |d - d^{GT}| + \frac{1}{chw} \sum |\hat{X} - X|, \quad (8)$$

where d and d^{GT} represent the estimated depth map and the ground truth (GT), \hat{X} and X represent the regression image and the underwater image. We set the hyperparameter $\lambda_1 = 3$ to balance the two losses. By adding the regression process in the training, d and X will be more closely structured.

In the second stage, we selected 1200 image pairs from the CYCLE [41] dataset, with 1080 pairs used for 100 epochs training and the remaining 120 pairs used for subsequent testing. To ensure the enhanced images with pleasing colors and details, we formulate the total loss L_s of DGEN using charbonnier loss and ssim loss. The former measures pixel similarity, while the latter evaluates structural similarity. The formula is as follows:

$$L_s = \sqrt{|x - y|^2 + \varepsilon^2} + \lambda_2(1 - \text{SSIM}(x, y)), \quad (9)$$

where x and y are the enhanced image and GT. λ_2 and ε are the hyperparameters for balancing losses, which were set to 0.5 and 10^{-3} , respectively.

IV. EXPERIMENT

A. Implementation Details

To assess the performance of UVZ, we use the remaining 120 image pairs from CYCLE dataset for comparison experiments. Additionally, we used four benchmark datasets: LNRUD [42], LSUI [43], UFO [44], and UIEB [9]. We randomly selected 500 images from LNRUD, 400 images from LSUI, 120 images from UFO, and 80 images from UIEB for more comprehensive testing.

The proposed model was trained and tested on NVIDIA GeForce RTX 2080 Ti GPUs using the PyTorch framework. We initialized the learning rate to 0.0002 and adjusted it gradually with Adam optimizer. For the CYCLE dataset, we measure the similarity between the enhanced results and the reference images by three common referenced metrics (i.e., PSNR, SSIM and MSE). For all datasets, we evaluate the performance by three no-reference metrics (i.e., UIQM [45], UICM and NIQE).

B. Comparison on reference dataset

Our UVZ was compared with some state-of-the-art methods, including four traditional methods (i.e., L^2 UWE [5], CBM [6], TEBCF [7], WWPE [8]), four deep learning methods (i.e., Water-Net [9], SCNet [10], TACL [11], Spectroformer [14]), and two depth-related methods (i.e., USUIR [12], PUGAN [13]).

Fig. 6 shows the enhancement results of all methods on the CYCLE dataset. L^2 UWE and USUIR improve image contrast, but noticeable color deviations persist. CBM and Water-Net have corrected colors to some extent, but the enlarged

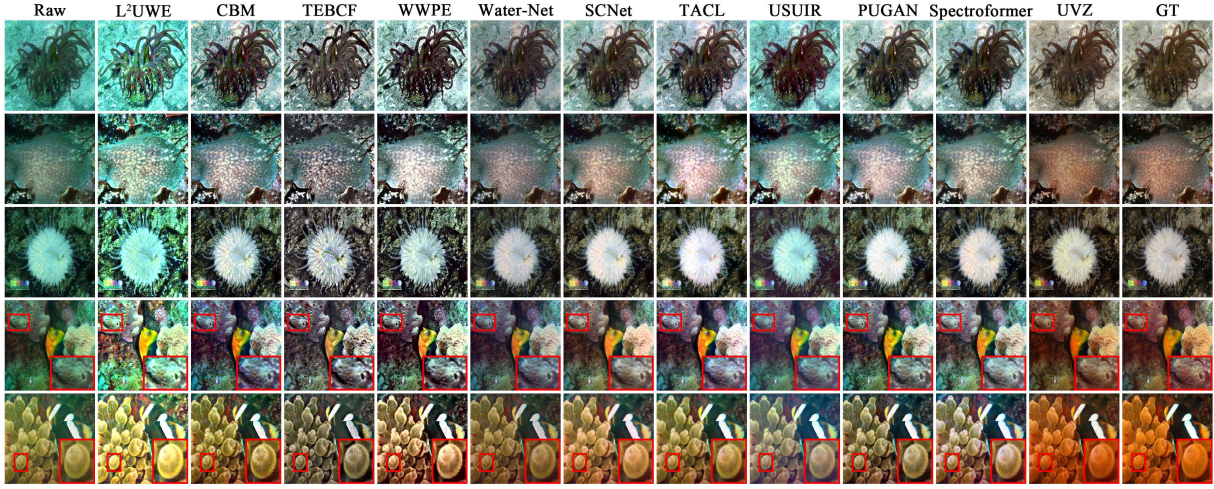


Fig. 6. Enhancement comparison on the CYCLE dataset. From left to right are the raw images, the results of L^2UWE [5], CBM [6], TEBCF [7], WWPE [8], and Water-Net [9], SCNet [10], TACL [11], USUIR [12], PUGAN [13], Spectroformer [14], the proposed UVZ, and the ground truth. The red box represents the enlarged details.

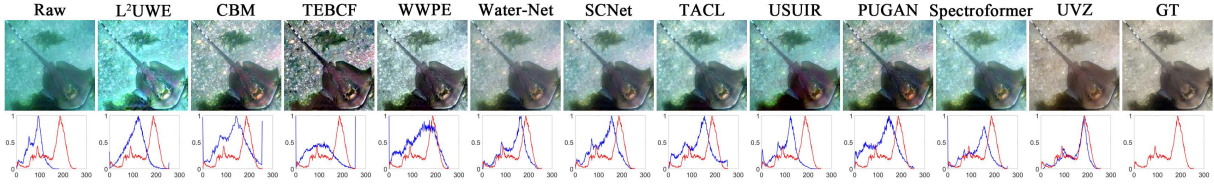


Fig. 7. Histogram comparison of red channel on the CYCLE dataset, with the raw image, the enhanced images from all methods, and GT on top, and the corresponding red channel histogram on bottom. The red and blue lines are the data distributions of the GT and enhanced images.

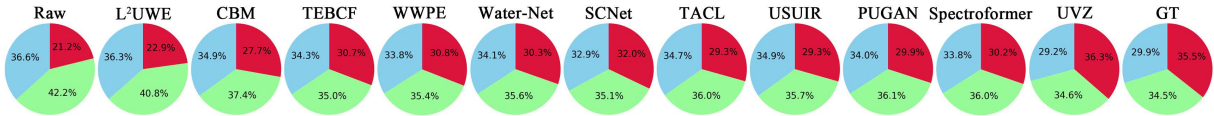


Fig. 8. Distribution comparison of RGB three-color on the CYCLE dataset

TABLE I
METRICS COMPARISON OF ALL METHODS ON THE CYCLE DATASET (OPTIMAL, SUB-OPTIMAL)

	L^2UWE	CBM	TEBCF	WWPE	Water-Net	SCNet	TACL	USUIR	PUGAN	Spectroformer	UVZ
PSNR \uparrow	14.55	21.48	18.74	17.40	<u>23.23</u>	22.48	21.78	20.55	21.43	21.42	26.00
SSIM \uparrow	0.6440	0.7461	0.6839	0.6412	<u>0.8196</u>	0.8116	0.7701	0.7739	0.7790	0.7910	0.8721
MSE \downarrow	0.06195	0.01745	0.02090	0.02560	0.01150	<u>4.629</u>	0.01597	0.02211	0.01571	0.01639	0.00435
UIQM \uparrow	2.634	4.151	4.606	4.291	4.573	<u>4.629</u>	4.444	4.321	4.522	4.332	5.044
UICM \uparrow	-76.35	-31.83	-13.71	-16.63	-16.43	<u>-11.01</u>	-23.29	-21.15	-20.74	-20.74	4.781
NIQE \uparrow	5.045	<u>6.548</u>	5.137	6.387	5.310	5.203	4.325	4.941	5.253	5.017	6.586
Runtime(s)	3.6725	0.2425	1.6340	0.3207	0.9613	0.0520	0.0595	0.0255	0.0488	<u>0.0394</u>	0.0583

image details are blurred. TEBCF significantly enhances the details of the image but results in darkened brightness and color confusion. WWPE, TACL, PUGAN, and Spectroformer alleviate the effects of color deviation, but enlarged details are still affected by blue-green. SCNet and our UVZ effectively eliminate color deviation and enhance image visibility, with the latter highlighting more vibrant colors. Moreover, we also exhibit the histograms of the red channel in Fig. 7, which is the most severely lost during underwater imaging. The curves of UVZ and GT overlap the most, indicating the closest

similarity. To further observe the color distribution, we show the pixel statistics on the RGB channels in Fig. 8. All methods enhance the degraded red channel to some extent, with UVZ being the most prominent. Its distribution on the red, green, and blue channels is 36.3%, 36.1%, and 29.2% respectively, which is more consistent with GT's 35.5%, 34.5%, and 29.9%.

Table I shows the quantitative comparison on the CYCLE dataset, where UVZ outperforms other state-of-the-art methods in all quality assessments, particularly with 11.9% and 8.9% performance improvements in PSNR and UIQM. Compared to other methods, Water-Net is more effective in removing color

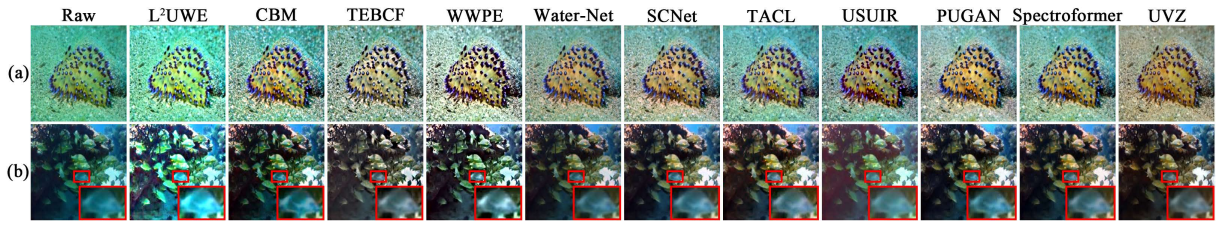


Fig. 9. Enhancement comparison of all methods on the LNRUD dataset

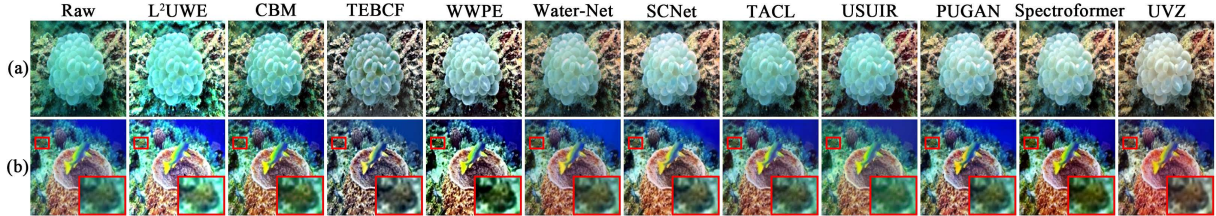


Fig. 10. Enhancement comparison of all methods on the LSUI dataset

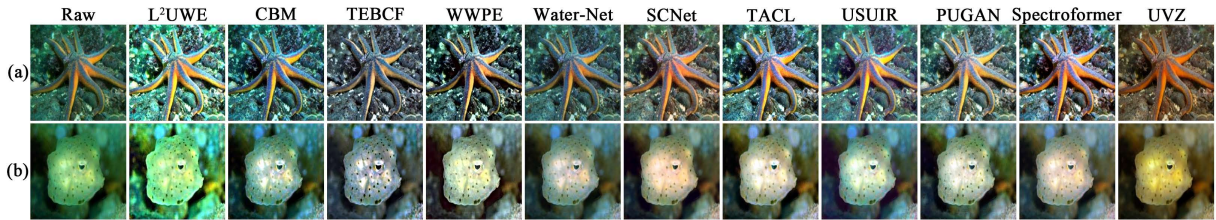


Fig. 11. Enhancement comparison of all methods on the UFO dataset

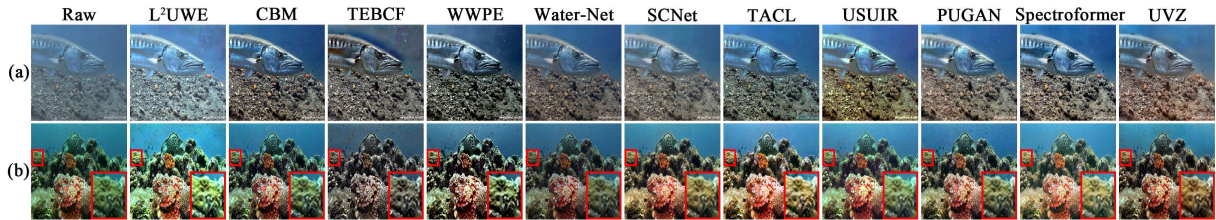


Fig. 12. Enhancement comparison of all methods on the UIEB dataset

deviation, while SCNet notably enhances the red channel. Therefore, these methods obtain most sub-optimal metrics in Table I. However, in terms of runtime, our method does not exhibit outstanding speed. To accurately guide region perception, UVZ adopts a two-stage design and multiple attentions. While these configurations require substantial computing resources, the model performance is nonetheless impressive.

C. Comparison on no-reference dataset

We present enhancement examples from LNRUD, LSUI, UFO and UIEB datasets in Figs. 9-12. In Fig. 9 (a) and Fig. 10 (a), the color enhancement from the UVZ is the most pronounced and well-established. While other methods mitigate the effects of color deviation, blue-green color still dominates the results. We enlarged the fishes in the near-far scenes in Fig. 9 (b) and Fig. 10 (b), respectively. It can see that only TEBCF and UVZ effectively remove the blue-green color, but the dull color of the former reduces the attractiveness.

From Fig. 11 and Fig. 12, it can be observed that L²UWE exhibits bright contrast enhancement, but over-exposure affects the color. The enhanced results of TEBCF, WWPE and Water-Net have low brightness and poor clarity. CBM effectively enhances image details, while TACL, USUIR and PUGAN alleviate the impact of color deviation. However, blue-green colors still dominate in their enhanced images. Despite the significant saturation increase in SCNet and Spectroformer, the enlarged far-view Fig. 12 (c) still shows deviated colors. Benefiting from its depth perception ability, our UVZ has excellent performance in terms of color, saturation, and visibility, whether in near or far scenes.

Table II gives the quantitative metrics on the above datasets, showcasing that our method excels in most metrics, especially the UICM representing the color metric. CBM exhibits impressive NIQE metrics, signifying a natural restoration of scene details. However, its color performance heavily affected the UICM evaluation.

TABLE II
METRICS COMPARISON OF ALL METHODS ON FOUR BENCHMARK DATASETS (OPTIMAL, SUB-OPTIMAL)

		L ² UWE	CBM	TEBCF	WWPE	Water-Net	SCNet	TACL	USUIR	PUGAN	Spectro-former	UVZ
LNRUD	UIQM↑	2.688	4.037	4.436	4.296	4.442	<u>4.452</u>	4.326	4.296	4.377	4.314	4.619
	UICM↑	-74.80	-31.29	<u>-16.69</u>	-17.15	-19.72	-16.85	-27.65	-21.25	-23.03	-20.33	-9.933
	NIQE↑	5.322	6.684	5.485	5.550	5.694	5.305	4.465	5.374	5.133	5.308	<u>6.241</u>
LSUI	UIQM↑	2.882	4.215	4.635	4.439	4.607	4.597	4.460	4.672	4.542	4.881	<u>4.863</u>
	UICM↑	-72.28	-29.06	-14.98	-13.64	-15.31	<u>-11.81</u>	-22.39	-20.31	-17.48	-15.64	-4.661
	NIQE↑	5.220	6.429	5.340	5.637	5.893	5.364	4.547	5.269	5.366	5.283	<u>6.006</u>
UFO	UIQM↑	2.800	3.849	4.223	4.325	4.283	4.998	4.047	4.116	4.209	4.109	<u>4.713</u>
	UICM↑	-68.97	-34.93	-20.31	-19.00	-21.88	<u>-17.00</u>	-33.61	-23.44	-26.55	-25.31	-2.238
	NIQE↑	4.385	4.398	4.808	4.575	4.707	<u>5.159</u>	4.520	4.924	5.081	5.046	6.322
UIEB	UIQM↑	2.716	3.911	4.240	4.505	<u>4.543</u>	4.427	4.390	4.474	4.487	4.384	4.896
	UICM↑	-73.48	-32.56	<u>-16.75</u>	-17.43	-20.36	-19.00	-23.79	-19.78	-21.79	-21.56	5.532
	NIQE↑	6.702	8.807	<u>6.977</u>	7.494	6.705	5.156	4.402	6.253	4.990	5.887	6.402

D. Ablation Study

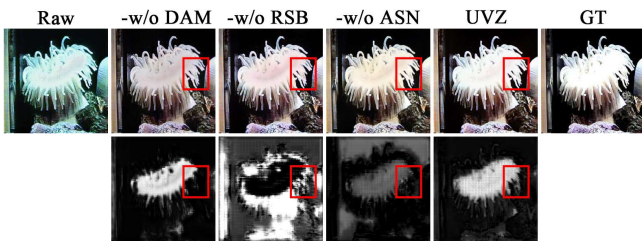


Fig. 13. Ablation comparison of the first stage configurations. The top shows the raw image, enhanced images for each configuration, and GT, and the bottom shows the estimated depth maps of the four configurations.

TABLE III
METRICS COMPARISON OF THE FIRST STAGE CONFIGURATIONS ON THE CYCLE DATASET (OPTIMAL, SUB-OPTIMAL)

	PSNR↑	MSE↓	UIQM↑	UICM↑	NIQE↑
-w/o DAM	25.73	0.00438	4.942	0.909	<u>6.500</u>
-w/o RSB	25.99	0.00437	<u>5.016</u>	<u>3.346</u>	6.371
-w/o ASN	26.00	0.00433	4.883	-0.952	6.410
UVZ	<u>26.00</u>	<u>0.00435</u>	5.044	4.781	6.586

We conducted a detailed ablation study for two stages separately. First, we removed different components in the first stage, and fixed the second stage configuration to train the entire network. The ablation configurations are as follows: (1) -w/o DAM, representing the removal of DAM in DEN, retaining only skip connections. (2) -w/o RSB, representing the removal of feature transmission from RSB in ASN. (3) -w/o ASN, representing the removal of auxiliary supervision from ASN in the training process. Fig. 13 compares the effects of the above configurations. In the absence of DAM, the depth estimation of scene details lacks accuracy, and the removal of RSB introduces confusion in the predicted depth. Therefore, the enhanced images of two configurations suffer from excessive red channel enhancement. The depth image of -w/o ASN deviates from the underwater image, leading to inaccurate color enhancement. In Table III, although the referenced metrics of the complete network are slightly lower

than that of -w/o ASN, the advantage of the no-reference metrics still proves a significant gain of ASN.

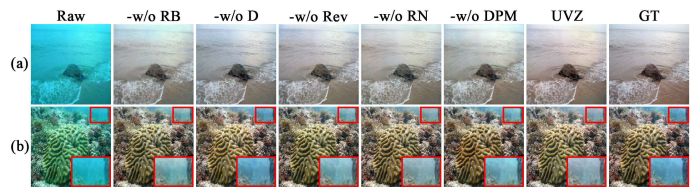


Fig. 14. Ablation comparison of the second stage configurations.

TABLE IV
METRICS COMPARISON OF THE SECOND STAGE CONFIGURATIONS ON THE CYCLE DATASET (OPTIMAL, SUB-OPTIMAL)

	PSNR↑	MSE↓	UIQM↑	UICM↑	NIQE↑
-w/o RB	25.62	0.00477	4.966	0.472	6.292
-w/o D	<u>25.76</u>	0.00448	5.024	3.613	6.474
-w/o Rev	25.73	0.00453	5.014	1.840	<u>6.504</u>
-w/o RN	25.69	0.00450	5.093	<u>4.733</u>	6.368
-w/o DPM	25.65	<u>0.00445</u>	5.020	4.478	6.277
UVZ	26.00	0.00435	<u>5.044</u>	4.781	6.586

Second, we fixed the configuration of the first stage, and removed different components in the second stage to obtain the following ablation network: (1) -w/o RB, representing the removal of all RB. (2) -w/o D, representing the removal of the depth maps in DPM, retaining only the second stage. (3) -w/o Rev, representing the removal of depth map reversal. (4) -w/o RN, representing the removal of RN in the R³N transformation, directing the local branch only through the reshaped depth map. (5) -w/o DPM, representing the removal of the DPM, retaining only skip connections. In Fig. 14. (a), the color of the complete network is the most consistent with GT. When the network lacks RB or DPM, the enhanced images are still affected by color deviation. While the red channel enhancement of -w/o D, -w/o Rev and -w/o RN is insufficient, and the color distribution of -w/o RN is chaotic. In the enlarged far water region of Fig. 14. (b), only the -w/o RN and the complete network effectively counter the color deviation.

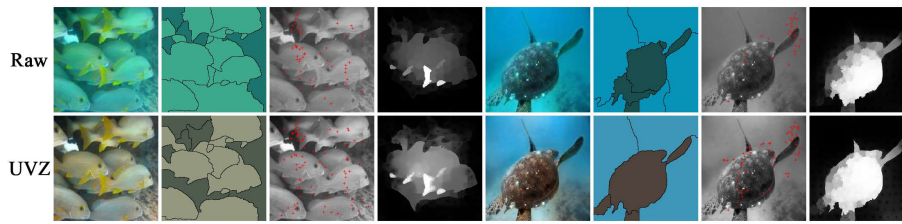


Fig. 15. Effect comparison of different tasks before and after enhancement. The top shows the raw images and task results, and the bottom shows the enhanced images and task results.



Fig. 16. Enhancement effects in different lighting environments. Our method can significantly improve the visibility without parameter adjustment.

E. Extended Applications

Without adjusting any parameters, we applied the model to three challenging tasks: image segmentation [46], keypoint detection [47], and saliency detection [48, 49], while also promoting it in low-light [50, 51] and exposure [52] scenarios. Fig. 15 illustrates the results of the different tasks. The enhanced image segmentation exhibits more accurate details, and the number of keypoints increases from 49 and 27 to 73 and 56, respectively. Additionally, the saliency structure of the image is also more specific. In Fig. 16, the UVZ effectively enhances the brightness and details of the low-light image, and makes the colors of the exposed image more vivid. The above good applications further validate the effectiveness and generalization of UVZ.

V. CONCLUSION

This paper proposes a novel UIE framework for depth-guided perception. In DEN, we use DAM to focus on regions with severe degradation, making the predicted depth map more reasonable. To ensure the relevance of depth map to scene, ASN is introduced into the training process to generate regression image. In addition, we design a DPM to capture near-far features, with the R³N transformation guiding the fusion of non-local and local branches. Extensive experiments on benchmark datasets demonstrate the advantages of our method and the gains of each module. Moreover, our method proves effectiveness across different visual tasks, improving visibility in challenging lighting conditions. In future work, we aim to optimize model efficiency and explore scenario enhancement by multiple semantic information.

ACKNOWLEDGMENTS

This work was supported by National Natural Science Foundation of China (61972064), LiaoNing Revitalization Talents Program (XLYC1806006) and the Fundamental Research Funds for the Central Universities (DUT19RC(3)012).

REFERENCES

- [1] S. Zhang, S. Zhao, D. An, D. Li, and R. Zhao, "Liteenhancenet: A lightweight network for real-time single underwater image enhancement," *Expert Systems with Applications*, vol. 240, p. 122546, 2024.
- [2] C. W. Park and I. K. Eom, "Underwater image enhancement using adaptive standardization and normalization networks," *Engineering Applications of Artificial Intelligence*, vol. 127, p. 107445, 2024.
- [3] W. Zhang, P. Zhuang, H.-H. Sun, G. Li, S. Kwong, and C. Li, "Underwater image enhancement via minimal color loss and locally adaptive contrast enhancement," *IEEE Transactions on Image Processing*, vol. 31, pp. 3997–4010, 2022.
- [4] Y. Guo, H. Li, and P. Zhuang, "Underwater image enhancement using a multiscale dense generative adversarial network," *IEEE Journal of Oceanic Engineering*, vol. 45, no. 3, pp. 862–870, 2019.
- [5] T. P. Marques and A. B. Albu, "L2uwe: A framework for the efficient enhancement of low-light underwater images using local contrast and multi-scale fusion," in *Proceedings of the IEEE/CVF Conference on Computer Vision and Pattern Recognition Workshops*, 2020, pp. 538–539.
- [6] J. Yuan, W. Cao, Z. Cai, and B. Su, "An underwater image vision enhancement algorithm based on contour bougie morphology," *IEEE Transactions on Geoscience and Remote Sensing*, vol. 59, no. 10, pp. 8117–8128, 2020.
- [7] J. Yuan, Z. Cai, and W. Cao, "Tebcf: Real-world underwater image texture enhancement model based on blurriness and color fusion," *IEEE Transactions on Geoscience and Remote Sensing*, vol. 60, pp. 1–15, 2022.
- [8] W. Zhang, L. Zhou, P. Zhuang, G. Li, X. Pan, W. Zhao, and C. Li, "Underwater image enhancement via weighted wavelet visual perception fusion," *IEEE Transactions on Circuits and Systems for Video Technology*, vol. 34, no. 4, pp. 2469–2483, 2024.
- [9] C. Li, C. Guo, W. Ren, R. Cong, J. Hou, S. Kwong, and D. Tao, "An underwater image enhancement benchmark dataset and beyond," *IEEE Transactions on Image Processing*, vol. 29, pp. 4376–4389, 2019.
- [10] Z. Fu, X. Lin, W. Wang, Y. Huang, and X. Ding, "Underwater image enhancement via learning water type desensitized representations," in *IEEE International Conference on Acoustics, Speech and Signal Processing*. IEEE, 2022, pp. 2764–2768.
- [11] R. Liu, Z. Jiang, S. Yang, and X. Fan, "Twin adversarial contrastive learning for underwater image enhancement and beyond," *IEEE Transactions on Image Processing*, vol. 31, pp. 4922–4936, 2022.
- [12] Z. Fu, H. Lin, Y. Yang, S. Chai, L. Sun, Y. Huang, and X. Ding, "Unsupervised underwater image restoration: From a homology perspective," in *Proceedings of the AAAI Conference on Artificial Intelligence*, vol. 36, no. 1, 2022, pp. 643–651.
- [13] R. Cong, W. Yang, W. Zhang, C. Li, C.-L. Guo, Q. Huang, and S. Kwong, "Pugan: Physical model-guided underwater image enhancement using gan with dual-discriminators," *IEEE Transactions on Image Processing*, vol. 32, pp. 4472–4485, 2023.

- [14] R. Khan, P. Mishra, N. Mehta, S. S. Phutke, S. K. Vipparthi, S. Nandi, and S. Murala, "Spectroformer: Multi-domain query cascaded transformer network for underwater image enhancement," in *Proceedings of the IEEE/CVF Winter Conference on Applications of Computer Vision*, 2024, pp. 1454–1463.
- [15] C. O. Ancuti, C. Ancuti, C. De Vleeschouwer, and P. Bekaert, "Color balance and fusion for underwater image enhancement," *IEEE Transactions on Image Processing*, vol. 27, no. 1, pp. 379–393, 2018.
- [16] S. An, L. Xu, I. Senior Member, Z. Deng, and H. Zhang, "Hfm: A hybrid fusion method for underwater image enhancement," *Engineering Applications of Artificial Intelligence*, vol. 127, p. 107219, 2024.
- [17] F. Alenezi, A. Armghan, and K. Santosh, "Underwater image dehazing using global color features," *Engineering Applications of Artificial Intelligence*, vol. 116, p. 105489, 2022.
- [18] J. Zhou, B. Li, D. Zhang, J. Yuan, W. Zhang, Z. Cai, and J. Shi, "Ugifnet: An efficient fully guided information flow network for underwater image enhancement," *IEEE Transactions on Geoscience and Remote Sensing*, vol. 61, pp. 1–17, 2023.
- [19] Y. Rao, W. Liu, K. Li, H. Fan, S. Wang, and J. Dong, "Deep color compensation for generalized underwater image enhancement," *IEEE Transactions on Circuits and Systems for Video Technology*, vol. 34, no. 4, pp. 2577–2590, 2024.
- [20] T. Chen, N. Wang, Y. Chen, X. Kong, Y. Lin, H. Zhao, and H. R. Karimi, "Semantic attention and relative scene depth-guided network for underwater image enhancement," *Engineering Applications of Artificial Intelligence*, vol. 123, p. 106532, 2023.
- [21] Y. Kang, Q. Jiang, C. Li, W. Ren, H. Liu, and P. Wang, "A perception-aware decomposition and fusion framework for underwater image enhancement," *IEEE Transactions on Circuits and Systems for Video Technology*, vol. 33, no. 3, pp. 988–1002, 2023.
- [22] D. Zhang, C. Wu, J. Zhou, W. Zhang, C. Li, and Z. Lin, "Hierarchical attention aggregation with multi-resolution feature learning for gan-based underwater image enhancement," *Engineering Applications of Artificial Intelligence*, vol. 125, p. 106743, 2023.
- [23] J. Zhou, Y. Wang, C. Li, and W. Zhang, "Multicolor light attenuation modeling for underwater image restoration," *IEEE Journal of Oceanic Engineering*, vol. 48, no. 4, pp. 1322–1337, 2023.
- [24] D. Berman, D. Levy, S. Avidan, and T. Treibitz, "Underwater single image color restoration using haze-lines and a new quantitative dataset," *IEEE Transactions on Pattern Analysis and Machine Intelligence*, vol. 43, no. 8, pp. 2822–2837, 2021.
- [25] A. Chandrasekar, M. Sreenivas, and S. Biswas, "Phish-net: Physics inspired system for high resolution underwater image enhancement," in *Proceedings of the IEEE/CVF Winter Conference on Applications of Computer Vision*, 2024, pp. 1506–1516.
- [26] Y. Wang, J. Guo, H. Gao, and H. Yue, "Uiec²-net: Cnn-based underwater image enhancement using two color space," *Signal Processing: Image Communication*, vol. 96, p. 116250, 2021.
- [27] N. Jiang, W. Chen, Y. Lin, T. Zhao, and C.-W. Lin, "Underwater image enhancement with lightweight cascaded network," *IEEE Transactions on Multimedia*, vol. 24, pp. 4301–4313, 2022.
- [28] D. Zhang, C. Wu, J. Zhou, W. Zhang, Z. Lin, K. Polat, and F. Alenezi, "Robust underwater image enhancement with cascaded multi-level sub-networks and triple attention mechanism," *Neural Networks*, vol. 169, pp. 685–697, 2024.
- [29] Y. Wang, S. Hu, S. Yin, Z. Deng, and Y.-H. Yang, "A multi-level wavelet-based underwater image enhancement network with color compensation prior," *Expert Systems with Applications*, vol. 242, p. 122710, 2024.
- [30] Q. Jiang, Y. Zhang, F. Bao, X. Zhao, C. Zhang, and P. Liu, "Two-step domain adaptation for underwater image enhancement," *Pattern Recognition*, vol. 122, p. 108324, 2022.
- [31] Z. Jiang, Z. Li, S. Yang, X. Fan, and R. Liu, "Target oriented perceptual adversarial fusion network for underwater image enhancement," *IEEE Transactions on Circuits and Systems for Video Technology*, vol. 32, no. 10, pp. 6584–6598, 2022.
- [32] K. Li, L. Wu, Q. Qi, W. Liu, X. Gao, L. Zhou, and D. Song, "Beyond single reference for training: underwater image enhancement via comparative learning," *IEEE Transactions on Circuits and Systems for Video Technology*, vol. 33, no. 6, pp. 2561–2576, 2023.
- [33] Q. Liu, X. Gao, L. He, and W. Lu, "Single image dehazing with depth-aware non-local total variation regularization," *IEEE Transactions on Image Processing*, vol. 27, no. 10, pp. 5178–5191, 2018.
- [34] M. Ju, C. Ding, C. A. Guo, W. Ren, and D. Tao, "Idrlp: Image dehazing using region line prior," *IEEE Transactions on Image Processing*, vol. 30, pp. 9043–9057, 2021.
- [35] Y. Yang, C. Wang, R. Liu, L. Zhang, X. Guo, and D. Tao, "Self-augmented unpaired image dehazing via density and depth decomposition," in *Proceedings of the IEEE/CVF Conference on Computer Vision and Pattern Recognition*, 2022, pp. 2037–2046.
- [36] J. Zhou, Q. Liu, Q. Jiang, W. Ren, K.-M. Lam, and W. Zhang, "Underwater camera: Improving visual perception via adaptive dark pixel prior and color correction," *International Journal of Computer Vision*, pp. 1–19, 2023.
- [37] G. Hou, N. Li, P. Zhuang, K. Li, H. Sun, and C. Li, "Non-uniform illumination underwater image restoration via illumination channel sparsity prior," *IEEE Transactions on Circuits and Systems for Video Technology*, vol. 34, no. 2, pp. 799–814, 2024.
- [38] Z. Liu, Y. Lin, Y. Cao, H. Hu, Y. Wei, Z. Zhang, S. Lin, and B. Guo, "Swin transformer: Hierarchical vision transformer using shifted windows," in *Proceedings of the IEEE/CVF International Conference on Computer Vision*, 2021, pp. 10012–10022.
- [39] T. Yu, Z. Guo, X. Jin, S. Wu, Z. Chen, W. Li, Z. Zhang, and S. Liu, "Region normalization for image inpainting," in *Proceedings of the AAAI Conference on Artificial Intelligence*, vol. 34, no. 07, 2020, pp. 12 733–12 740.
- [40] C. Li, S. Anwar, and F. Porikli, "Underwater scene prior inspired deep underwater image and video enhancement," *Pattern Recognition*, vol. 98, p. 107038, 2020.
- [41] C. Fabbri, M. J. Islam, and J. Sattar, "Enhancing underwater imagery using generative adversarial networks," in *IEEE International Conference on Robotics and Automation*. IEEE, 2018, pp. 7159–7165.
- [42] T. Ye, S. Chen, Y. Liu, Y. Ye, E. Chen, and Y. Li, "Underwater light field retention: Neural rendering for underwater imaging," in *Proceedings of the IEEE/CVF Conference on Computer Vision and Pattern Recognition*, 2022, pp. 488–497.
- [43] L. Peng, C. Zhu, and L. Bian, "U-shape transformer for underwater image enhancement," *IEEE Transactions on Image Processing*, vol. 32, pp. 3066–3079, 2023.
- [44] M. J. Islam, P. Luo, and J. Sattar, "Simultaneous enhancement and super-resolution of underwater imagery for improved visual perception," *arXiv preprint arXiv:2002.01155*, 2020.
- [45] K. Panetta, C. Gao, and S. Agaian, "Human-visual-system-inspired underwater image quality measures," *IEEE Journal of Oceanic Engineering*, vol. 41, no. 3, pp. 541–551, 2015.
- [46] T. Lei, X. Jia, Y. Zhang, S. Liu, H. Meng, and A. K. Nandi, "Superpixel-based fast fuzzy c-means clustering for color image segmentation," *IEEE Transactions on Fuzzy Systems*, vol. 27, no. 9, pp. 1753–1766, 2018.
- [47] D. G. Lowe, "Distinctive image features from scale-invariant keypoints," *International Journal of Computer Vision*, vol. 60, pp. 91–110, 2004.
- [48] C. Li, Y. Yuan, W. Cai, Y. Xia, and D. Dagan Feng, "Robust saliency detection via regularized random walks ranking," in *Proceedings of the IEEE/CVF Conference on Computer Vision and Pattern Recognition*, 2015, pp. 2710–2717.
- [49] Y.-f. Zhang, J. Zheng, L. Li, N. Liu, W. Jia, X. Fan, C. Xu, and X. He, "Rethinking feature aggregation for deep rgb-d salient object detection," *Neurocomputing*, vol. 423, pp. 463–473, 2021.
- [50] C. Lee, C. Lee, and C.-S. Kim, "Contrast enhancement based on layered difference representation of 2d histograms," *IEEE Transactions on Image Processing*, vol. 22, no. 12, pp. 5372–5384, 2013.
- [51] C. Xu, H. Fu, L. Ma, W. Jia, C. Zhang, F. Xia, X. Ai, B. Li, and W. Zhang, "Seeing text in the dark: Algorithm and benchmark," *arXiv preprint arXiv:2404.08965*, 2024.
- [52] V. Bychkovsky, S. Paris, E. Chan, and F. Durand, "Learning photographic global tonal adjustment with a database of input/output image pairs," in *Proceedings of the IEEE/CVF Conference on Computer Vision and Pattern Recognition*. IEEE, 2011, pp. 97–104.